

Single phase multifunctional integrated converter for electric vehicles

Kondreddy Sreekanth Reddy, Sreenivasappa B. Veeranna

Center for Research in Power Electronics, Presidency University, Bengaluru, India

Article Info

Article history:

Received Jun 7, 2021

Revised Sep 24, 2021

Accepted Oct 6, 2021

Keywords:

Electric vehicle

Induction motor drive

Integrated converter

Single phase charging

ABSTRACT

In this paper, a single phase multifunctional integrated converter is proposed for electric vehicles (EVs) with single stage power conversion. The main objective of the proposed topology is to reduce the weight, size, and cost of the power electronic converter system used in EVs compared to the existing topologies that are already available in the industries. The novelty of the proposed topology includes: (i) single converter for charging, propulsion and regenerative braking; (ii) reduction of number of switches to reduce the switching and conduction losses; (iii) improving the efficiency by reducing the value of inductor; (iv) power factor correction for AC grid; and (v) improving the total harmonic distortion of the grid current. The complete analysis of the various modes of operation of the proposed topology is analyzed and implemented through MATLAB/Simulink software simulation and a power factor of 0.9999 and a current total harmonic distortion (THD) of 2.16% is achieved. The proposed topology is also compared with the existing topologies in terms of number of switches, diodes, inductors and capacitors used.

This is an open access article under the [CC BY-SA](https://creativecommons.org/licenses/by-sa/4.0/) license.



Corresponding Author:

Kondreddy Sreekanth Reddy

Center for Research in Power Electronics

Presidency University

Rajankunte, Yelahanka, Bengaluru, India

Email: ksreekanthreddy@presidencyuniversity.in

1. INTRODUCTION

The demand for fossil fuel is ever increasing and dependency of fuel on other countries leads to increase in price and shortage of fuel in nearby future have caused a major change from internal combustion engine vehicles to electric vehicles (EVs) for the transportation purpose. The EVs are becoming more popular because of the existence of power electronic converter systems, which provide zero emission, less noise, smooth operation, high efficiency, independency of petroleum fuels and easy control. The important components of EVs are charger, motor and energy system. Based on the type of charging, chargers are classified as onboard and off board chargers. Though the off-board charger has the fastest charging capability, the drawbacks such as requirement of large infrastructure and charging time constraints are the limiting factors for the usage of off board chargers [1], [2]. In order to overcome the limitations of off board charger, presently many EVs are fitted with semi-fast onboard charger (OBC) for charging the batteries [3]-[5]. There are numerous approaches of OBC topologies, in which the best collective method used in recent times is the integrated OBC chargers to overcome the drawbacks of conventional OBC chargers such as low power charging capacity, heavy weight and space constraints [6]-[11]. In integrated converter common topology is used for battery charging as well as to drive the traction motor [12], [13]. A compact weightless bidirectional direct current to direct current (DC/DC) integrated converter is proposed

for acceleration and cruising in [14]. In [14] the charging and propulsion are not happening at the same time because of the common power stage between bidirectional DC/DC converter and charger. In [15], integrating the resonant inductor into the transformer confirms that the limited liability company (LLC) resonant converter decreases its volume which is particularly suitable as integrated onboard charger for EV. But the paper doesn't explain about the imbalance of leakage inductance which is quite common in center tapped transformer with bifilar winding and change in parameters under the presence of resonant inductor. The cause for the difference in imbalance of leakage inductance is clearly explained in [16]. In [16], precise circuit model of LLC integrated converter is presented with clear explanation for the cause of change in parameters under influence of resonant frequency along with the equal turning ratio at the secondary side of center tapped transformer. Though there is improvement in one aspect but the cost and space are becoming more due to the presence of two stage conversion. In [17], though a common topology is proposed to achieve charging, propulsion and regenerative braking, but during any mode of operation three to four switches will be in ON position, this increases the cost and losses of the converter. In [18] a new integrated bidirectional ac/dc converter with four switches, four diodes and two inductor elements is proposed. The features of the paper are 2 to 2.5% efficiency improvement in boost mode and the second inductor size is reduced comparatively from single inductor converters. But the authors are not clearly explained the design methodology of the inductors L1 and L2, in addition to this the authors are claiming that the size of the inductor is reduced by 35-40% but the details are not included in the paper. Having two inductors the authors are claiming that the proposed converter has least inductor value compare to the existing topology proposed in [17], with single inductor whose value is 770 μH which is very much smaller than two inductors whose values are 3 mH each. In the existing topology proposed in [18], the range of duty cycle is not clearly mentioned during regenerative braking boost mode at low speed. Therefore, the boost operation for all the operating condition may not be possible, especially at very low speed. In addition to the above, the cost and size of the converter is still high due to the presence of four switches and two inductors. In the present paper, a single phase multifunctional integrated converter is proposed with only three switches and two inductor elements of lower value by achieving all the operating modes of EVs with design analysis of inductor. The present paper also discusses on the operation of regenerative braking buck mode with ($V_h \geq V_b$). It means, during regenerative braking mode the converter is designed to operate at a speed greater than or equal to threshold speed.

The paper is structured as follows: in section 2, the description of the proposed topology and modes of operation are explained. Section 3 discusses, the complete control algorithm techniques. The MATLAB simulation results are given in section 4 and the conclusions are outlined in section 5.

2. PROPOSED TOPOLOGY AND MODES OF OPERATION

The proposed multifunctional integrated converter is shown in Figure 1, that includes three active switches (S_1-S_3) with body diodes (D_5, D_7 and D_8), a bridge rectifier with four diodes (D_1-D_4), two inductors (L_1-L_2), three capacitors (C_1-C_3) and a diode (D_6). The passive elements are used as filter to suppress the ripple from the bridge rectifier so that pure DC can be supplied to the battery while charging.

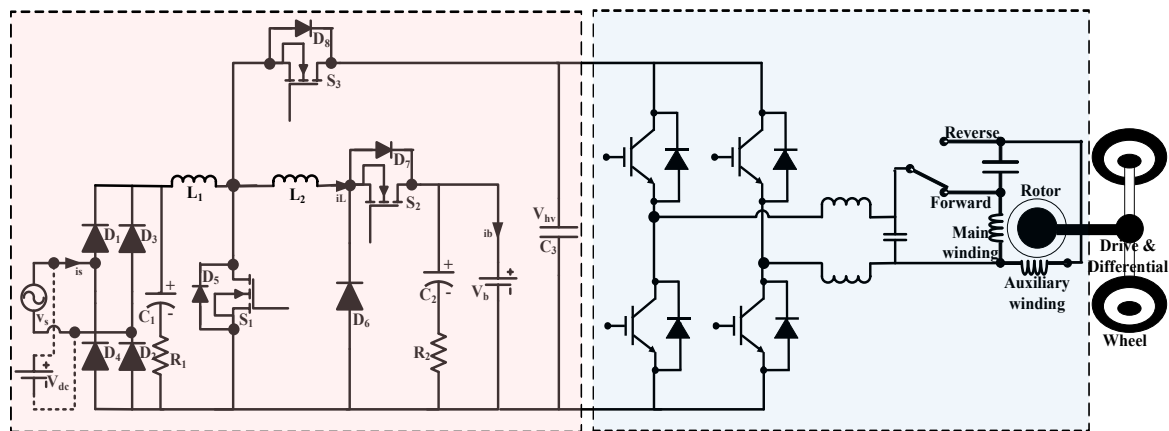


Figure 1. Proposed multifunctional integrated converter

The proper selection of the ON and OFF switches with the combined elements will provide different modes of operation, such as plug-in charging, buck propulsion, boost propulsion and regenerative braking. The switching states of the proposed topology in various modes are indicated in Table 1 and the modes of operations are analyzed through continuous conduction mode (CCM).

Table 1. Switching states of proposed topology in various modes

Mode of operation	S1	S2	S3	Conducting Diodes
Plug in Mode	PWM	OFF	OFF	D ₇ -ON
Propulsion Buck mode	OFF	PWM	OFF	D ₈ -ON
	OFF	PWM	OFF	D ₆ -ON
Propulsion Boost Mode	PWM	ON	OFF	D ₈ -ON
Regenerative Breaking mode	OFF	OFF	PWM	D ₇ -ON
	OFF	OFF	PWM	D ₅ -ON

2.1. Plug-in charging mode

In plug-in charging mode shown in Figure 2, the charger plug is connected to either AC source supply (low and medium level charging) or DC source supply (fast charging) socket for charging the battery. The charging time of the battery depends on the battery capacity and the amount of charging power supplied. In the existing topology [11] during the plug-in charging mode the converter always operates in boost mode with a different duty cycle, which means that output voltage is always greater than or equal to the rectified voltage. In the present paper, the input supply is selected in such a way as to obtain the required battery voltage after filtering the rectified voltage with the help of the filter $C_1-(L_1 + L_2)-C_2$ with damping resistors R_1 and R_2 . This prevents the compulsion to operate the converter in boost mode during plug-in charging, thus minimizing switching and conduction losses.

$$T_{Charge} [h] = \frac{\text{Battery Capacity [kWh]}}{\text{Charging Power [kW]}} \quad (1)$$

In the filter $C_1-(L_1 + L_2)-C_2$, major filtering is done with the help of capacitor C_1 which is designed to offer very low reactance. The remaining filtering is done by the combination of $(L_1 + L_2)$ and C_2 . The transfer function for $C_1-(L_1 + L_2)-C_2$ filter with damping resistors R_1 and R_2 is given by the (2).

$$G_f(s) = \frac{i_b(s)}{i_s(s)} = \frac{s^2 R_1 C_1 C_2 + s C_2}{s^3 (L_1 + L_2) C_1 C_2 + s^2 (R_1 + R_2) C_1 C_2 + s (C_1 + C_2)} \quad (2)$$

$$R_1 = \frac{1}{3} X_{C1} \quad \text{where} \quad X_{C1} = \frac{1}{2\pi f_{C1} C_1} \quad \text{and} \quad f_{C1} = 100\text{Hz}$$

$$R_2 = \frac{1}{3} X_{C2} \quad \text{where} \quad X_{C2} = \frac{1}{2\pi f_{C2} C_2} \quad \text{and} \quad f_{C2} = \frac{1}{2\pi\sqrt{(L_1 + L_2)C_2}}$$

The magnitude and phase plot comparison of $C_1-(L_1 + L_2)-C_2$ filter is given in Figure 3, it is clear from the plot that both magnitude and phase response of the filter is improving in the presence of passive damping resistors R_1 and R_2 for the frequencies greater than 10kHz . The current path in this mode is $|v_s| - L_1 - L_2 - D_7 - V_b - |v_s|$

For a given battery voltage the voltage conversion ratio (m_1) in this mode is related through the

$$m_1 = \frac{V_b}{|v_s|} = \frac{1}{1-d_1} \quad (3)$$

The duty cycle d_1 is controlled to obtain the required battery voltage.

2.2. Propulsion buck mode

In this mode power transfer takes place from the battery to the DC link capacitor by operating switch S_2 in PWM mode. The switching and associated waveforms as shown in Figure 4 includes battery voltage, PWM pulses for S_2 switch, DC link voltage, current through the inductor L and diode D_6 . The equivalent circuit when S_2 is ON and when S_2 is OFF are shown in Figures 5(a) and 5(b) respectively.

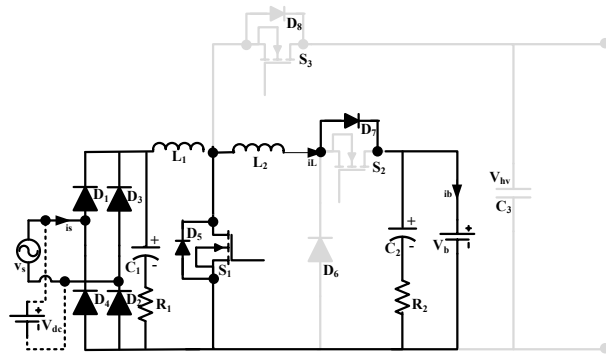


Figure 2. Equivalent circuit in plug-in charging mode

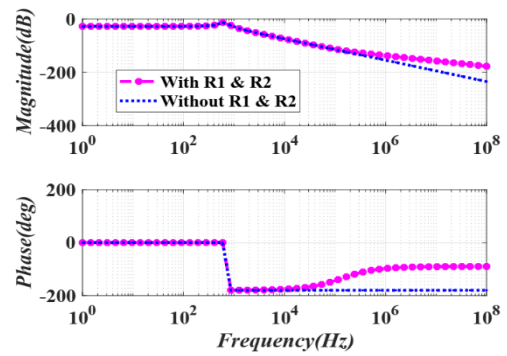


Figure 3. Magnitude and phase plot of $C_1-(L_1 + L_2)-C_2$ filter with and without passive damping resistors R_1 and R_2

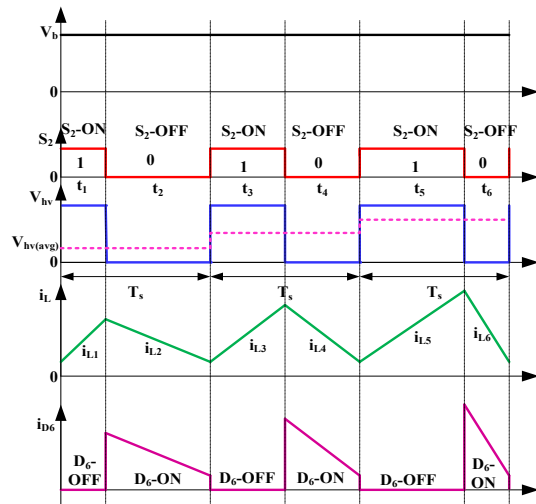


Figure 4. Switching waveforms in propulsion buck mode

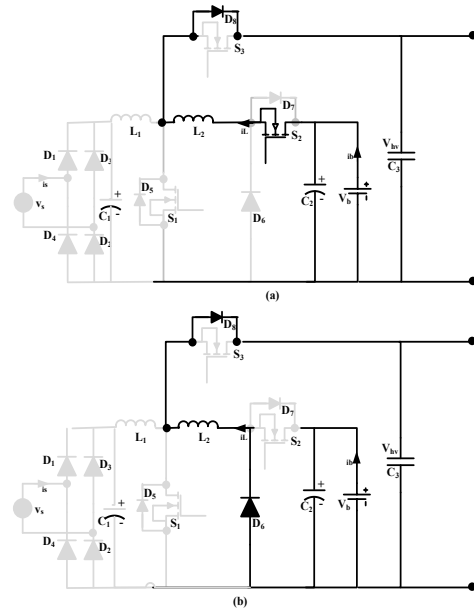


Figure 5. Equivalent circuit in propulsion buck mode (a) S_2 is ON and (b) S_2 is OFF

The battery supplies energy to the inductor L_2 and to the load, when S_2 is ON through the path $V_b - S_2 - L_2 - D_8 - C_3 - V_b$. When S_2 is OFF, the inductor transfers its energy to the load through the path $L_2 - D_8 - C_3 - D_6 - L_2$. The duty cycle in this mode is d_2 and the voltage conversion ratio m_2 are related through the (4).

$$m_2 = V_{hv} = d_2 \times V_b \tag{4}$$

The value of d_2 is decided by the acceleration and load capacity (light load condition).

2.3. Propulsion boost mode

In this mode, boost operation is obtained with the help of $C_2, S_2, S_1, L_2, D_8, C_3$ as shown in Figures 6(a) and 6(b) and the corresponding switching waveforms are shown in Figure 7. Switch S_1 is operated in PWM mode and switch S_2 is continuously ON. When S_1 is turned ON the inductor stores energy through the path $V_b - S_2 - L_2 - S_1 - V_b$ and when S_1 is turned OFF the inductor transfers energy to the DC link capacitor C_3 through the path $V_b - S_2 - L_2 - D_8 - C_3 - V_b$. The duty cycle for this mode be d_3 and voltage conversion ratio m_3 are related through the (5).

$$m_3 = V_{hv} = \frac{V_b}{1-d_3} \tag{5}$$

The average current through the inductor is expressed as (6).

$$i_{Lavg} = \frac{1}{2T_s} \left[\int_0^{T_s} i_L(t) dt \right] \tag{6}$$

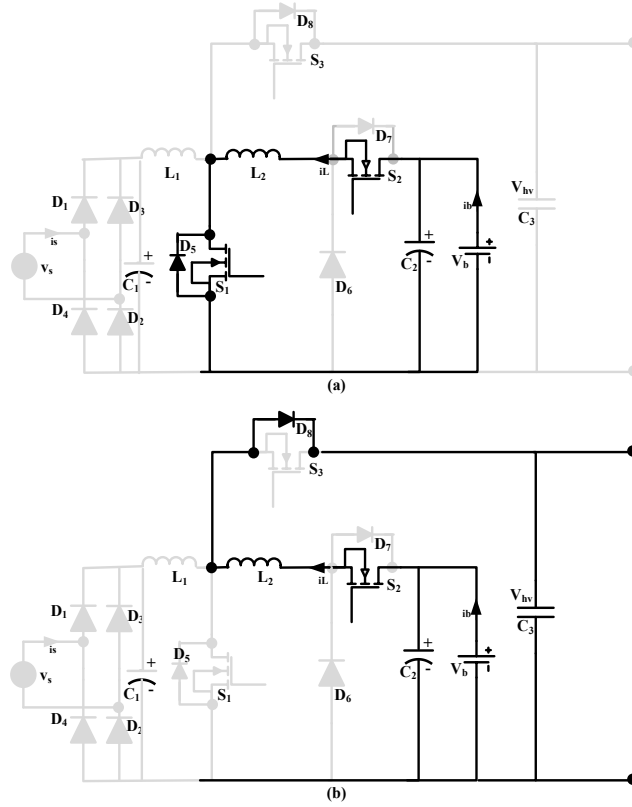


Figure 6. Equivalent circuit in propulsion boost mode (a) S_1 is ON and (b) S_1 is OFF

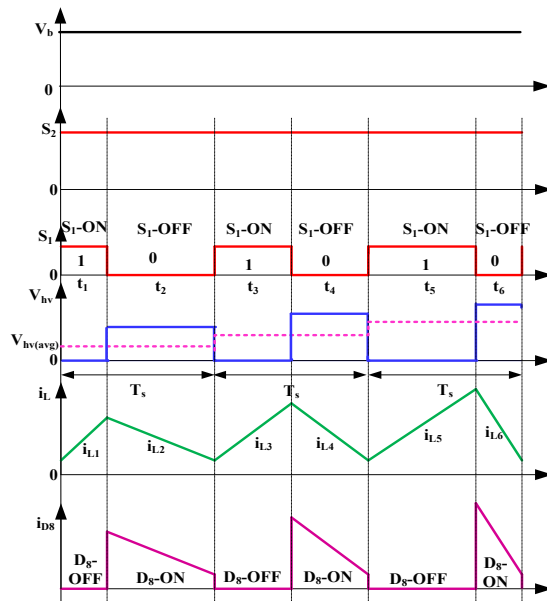


Figure 7. Switching waveforms in propulsion boost mode

2.4. Regenerative braking mode

When the motor drive inverter produces energy during regenerative braking, due to which the DC link voltage increases. The charging of the battery is done from the developed high DC link voltage by operating the converter in regenerative buck mode as shown in Figure 8. In this mode, buck converter operation is achieved by $C_3, S_3, L_2, D_7, C_2,$ and D_5 . During regenerative braking when switch S_3 is turned ON, the DC link voltage supplies energy to the inductor through the path $C_3 - S_3 - L_2 - D_7 - V_b - C_3$ as shown in Figure 8(a). When switch S_3 is turned OFF, the energy stored in the inductor transfer to the battery through the path $L_2 - D_7 - V_b - D_5 - L_2$ as shown in Figure 8(b). In Figure 9 the corresponding switching waveforms of regenerative braking mode are shown.

Let the duty cycle in this mode be d_4 and the voltage conversion ratio m_4 are related through the (7).

$$m_4 = V_b = d_4 \times V_{hv} \tag{7}$$

In this mode, the boost operation is avoided because when the vehicle is running at very low speed the amount of voltage generated during braking may not be sufficient to charge the battery. Hence, during braking the converter is operated in buck mode by operating the switch S_3 in PWM mode, so that required voltage by the battery can be obtained when the vehicle is running at a speed greater than or equal to certain threshold level corresponds to $(V_{hv} \geq V_b)$.

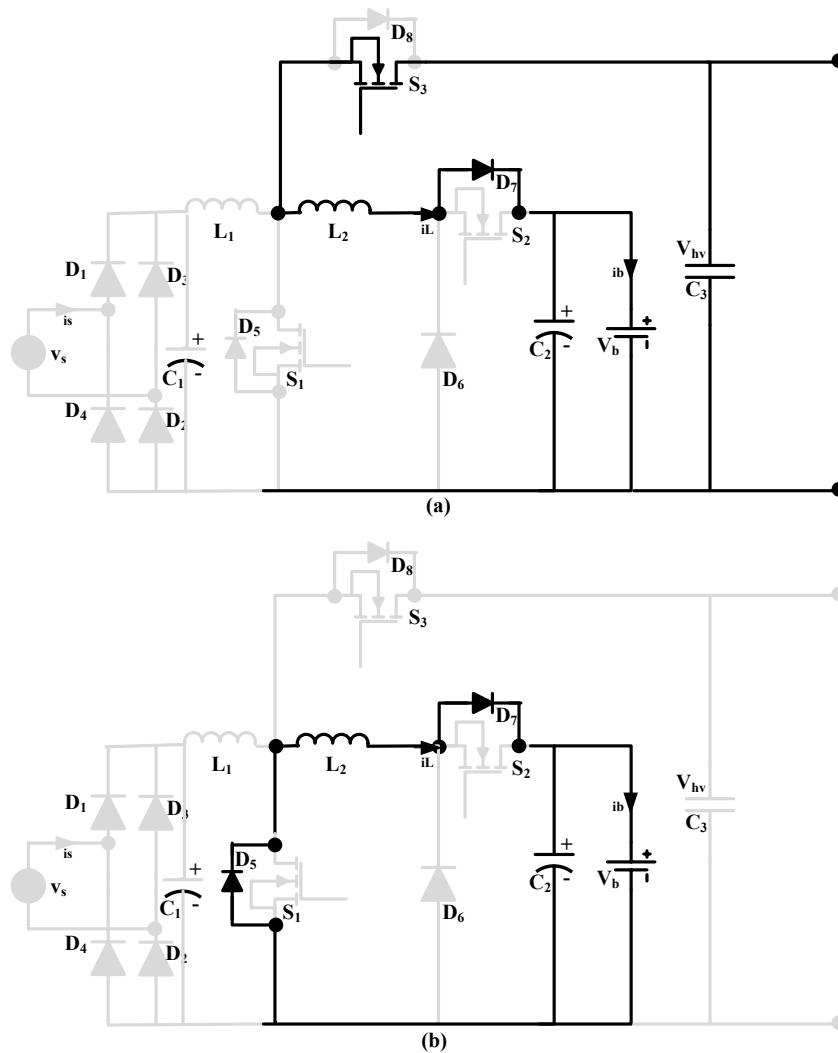


Figure 8. Equivalent circuit in regenerative braking mode (a) S_3 is ON and (b) S_3 is OFF

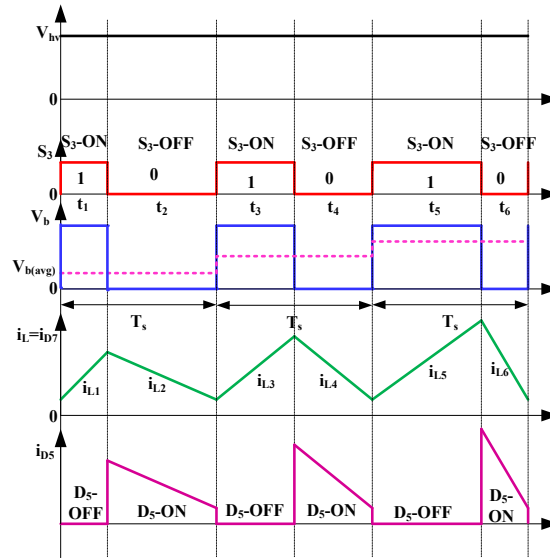


Figure 9. Switching waveforms in regenerative buck mode

3. DESIGN ANALYSIS AND CONTROL TECHNIQUES

3.1. Design analysis

In this section the parameters needed for selecting the switching and passive elements are briefly explained.

a) Selection of switches and diodes

The selection of a particular semiconductor switch and diode is based on voltage, current and power ratings for each operating mode. In the proposed topology. The peak voltage rating of S_1 and S_2 is based on maximum battery voltage $VS_{1P} = VS_{2P} = \max(|v_s|, V_b)$ and the peak voltage rating of S_3 is based on the maximum DC link voltage. The voltage rating of diode D_6 is based on $\max(V_{hv}, V_b)$. The peak current rating of S_1 and S_2 is based on peak battery current and the peak current rating of S_3 is based on the peak DC link current. The current rating of diode D_6 is based on $\max(I_{hv}, I_b)$.

b) Selection of the inductor

Based on the given specification, the selection of the inductor L_1 is based on switching frequency f_s and filter capacitor C_2 .

$$L_1 = \frac{1}{4\pi^2 f_s^2 C_2} \tag{8}$$

The inductor L_2 is calculated based on current ripple approximation and as a function of switching frequency f_s .

$$L_2 = \frac{\sqrt{2}V_s}{4f_s \Delta I_L (pk-pk)} \tag{9}$$

c) Selection of the Capacitors

In the proposed converter three capacitors C_1 at the output of bridge rectifier, C_2 across the battery and C_3 at the high DC link voltage side are connected as shown in Figure 1. The designing equations for these capacitors are expressed as:

$$C_1 = \frac{1}{4\sqrt{3}fR_b\gamma} \tag{10}$$

$$C_2 = \frac{V_b}{4f_s R_b \Delta V_b} \tag{11}$$

$$C_3 = \frac{V_{hv}}{4f_s R \Delta V_{hv}} \tag{12}$$

4. CONTROL TECHNIQUES

The control technique for the proposed topology in plug-in charging mode, propulsion boost mode, propulsion buck mode and regenerative braking mode are shown in Figure 10, Figure 11 Figure 12 and Figure 13 respectively. The [19]-[24] discusses various controlling techniques for converters used in EV applications. The control technique inputs for the proposed topology is selected based on the external feedback signals taken from dc link voltage, battery voltage, speed and torque. In plug-in charging mode two proportional, integral, derivative (PID) controllers (inner loop and outer loop) are used as shown in Figure 10. The inner PID controller with a transfer function $G_{pid_{ib}}(Z) = K_p \left[1 + \frac{T_s}{T_i(Z-1)} + T_d \frac{(Z-1)}{T_s} \right]$ regulates the battery current and outer PID controller with a transfer function $G_{pid_{gb}}(Z)$ regulates the battery voltage. The AC grid voltage is attenuated with the help of a transformer and a resistive network to obtain the required AC voltage. This AC voltage is converted to equivalent reference DC voltage V_g using a rectifier and a filter.

The voltage V_g is compared with the measured battery voltage V_b to get the error signal. This error signal is fed to the input of outer PID controller to generate reference battery current I_b^* which is compared with the measured battery current I_b to get error signal which is required for the inner PID controller to generate controlled step signal. The step signal is compared with the high frequency saw tooth signal to get pulse width modulated (PWM) signal to drive the switch S_1 in PWM mode. The selector switch selects a particular switch to operate either in PMW mode or in ON/OFF mode. In this control technique, selector switch selects S_1 switch to operate in PWM mode, by keeping switches S_2 and S_3 in OFF mode. The propulsion boost mode consists of inner loop and outer loop PID controllers as shown in Figure 11. The inner PID controller with a transfer function $G_{pid_{ib}}(Z)$ regulates the battery current and outer PID controller with a transfer function $G_{pid_{hv}}(Z)$ regulates the DC link voltage. The speed is converted to equivalent reference DC link voltage using speed to voltage converter to get reference DC link voltage V_{hv}^* , this voltage is compared with the measured DC link voltage V_{hv} to get the error signal. This error signal is given to the input of outer PID controller to generate reference battery current I_b^* which is compared with the measured battery current I_b to get error signal which is given as an input of inner PID controller to generate controlled step signal. The step signal is compared with the high frequency saw tooth signal to get pulse width modulated (PWM) signal to drive the switch S_1 in PWM mode. In this technique, selector switch selects the switch S_1 to operate in PWM mode, switch S_2 in ON mode and switch S_3 in OFF mode. The control technique for propulsion in buck mode is shown in Figure 12 is similar to propulsion in boost mode except the switching combinations selected by selector switch. The selector switch keeps switch S_2 in PWM mode, switch S_1 and S_3 in OFF mode.

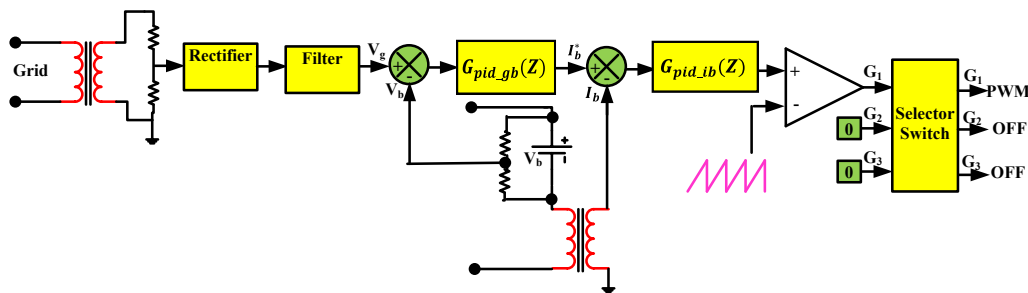


Figure 10. Control technique in plug-in charging mode

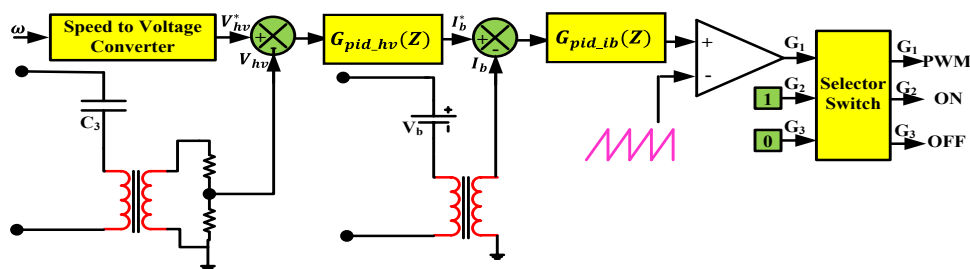


Figure 11. Control technique in propulsion boost mode

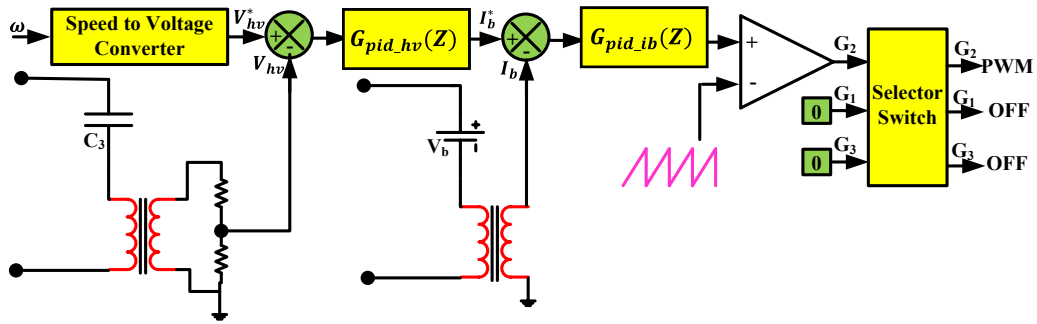


Figure 12. Control technique in propulsion buck mode

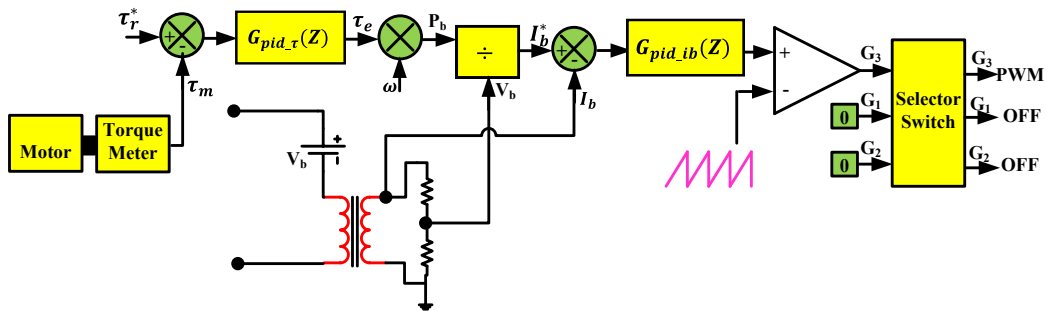


Figure 13. Control technique in regenerative braking mode

The control technique for regenerative braking mode is shown in Figure 13 that consists of two PID controllers. The inner PID controller with a transfer function $G_{pid_ib}(Z)$ regulates the battery current and outer PID controller with a transfer function $G_{pid_τ}(Z)$ regulates the torque of the motor. The motor torque is measured through torque meter to get measured torque τ_m , this is compared with the reference torque τ_r^* (reference torque is obtained by dividing battery power by speed i.e. $\tau_r^* = P_b/\omega$) to get the error signal. This error signal is given to the input of outer PID controller to generate step equivalent of error torque τ_e which is multiplied by speed to get P_b . The battery power P_b is divided by V_b to get reference battery current I_b^* , this current is compared with measured I_b to get error signal. The error signal is given to the input of inner PID controller to generate controlled step signal. The step signal is compared with the high frequency saw tooth signal to get pulse width modulated (PWM) signal to drive the switch S_3 in PWM mode. The selector switch keeps switch S_3 in PWM mode, switch S_1 and S_2 in OFF mode. The complete tuning of the PID controller is done with the help of frequency sampling auto tuning method in Simulink.

5. RESULTS AND DISCUSSION

This section presents the results and discussions of the proposed topology. The simulation of the proposed topology has been verified using MATLAB/Simulink tool with version R2017a for the specifications given in Table 2. The active and passive components, measurement blocks and sources are selected from Sim-Power systems tool box. The blocks required (constant, multiplier, addition, gain, and source) for the implementation of control technique are selected from Simulink tool box. The model configuration parameters are selected as follows: start time=0.0s, stop time=0.1s, solver type is fixed step, solver is automatic solver selection, fixed step size of 1e-6s. The simulations result during charging mode, propulsion buck mode, propulsion boost mode and regenerative braking mode are shown in Figures 14 to 20. In charging mode, the battery can be charged either from AC source or from DC source. In Figure 14 source voltage, source current, rectified voltage after full wave rectification, battery voltage and battery current are included at 100% battery charge voltage of 400V with AC source voltage of 220V. The input power is maintained at 1kW between 0.5 to 1 sec, and from 1sec to 1.5sec it is increased to 1.2kW and from 1.5 to 2 sec it is reduced back to 1kW again. The input power factor is measured with the help of Simulink power factor measurement block and found to be equal to 0.9999. The current THD (I_{THD}) is calculated by taking FFT for one cycle data during steady state condition and found to be equal to 2.16%.

Table 2. Parameters and specifications

Parameters	Specifications
Grid voltage (V_s)	220 V
Grid frequency (f)	50 Hz
Battery Power (P_b)	1 kW
Battery Voltage (V_b)	400 V
DC link voltage (V_{hv})	400 V
Switching frequency (f_s)	20 kHz
Inductor (L_1)	1 mH
Inductor (L_2)	598.32 μ H
Filter Capacitor (C_1)	100 μ F
Battery Capacitor (C_2)	2200 μ F
DC link Capacitor (C_3)	220 μ F

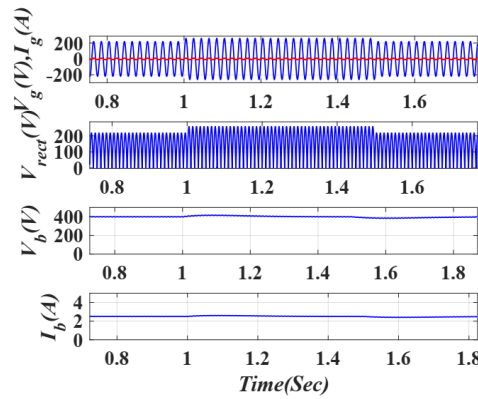


Figure 14. Waveforms during charging mode at 100% battery charge from AC Zoomed version of the waveforms and voltage (blue color) and I_g (red color) waveforms are included

The harmonic spectrum of grid voltage and grid current are included in the Figure 15. In Figure 16 source Voltage, source current, rectified voltage (same as DC source voltage), battery voltage and battery current are included with DC source voltage equal to 400V. The associated waveforms during propulsion buck mode with step change in the DC link voltage is obtained by changing duty cycle of the switch S_2 to attain the required speed are given in Figure 17. The waveforms associated during propulsion buck mode for low-speed condition with variable load are given in Figure 18 to verify the response of the proposed converter against the change in load. It is clear from the DC link voltage waveform in Figure 19 that the response time of the converter against change in the speed to achieve steady state output is around 15ms between 0 to 0.05s, 25ms between 0.05 to 0.1s and 40ms between 0.1 to 0.15s.

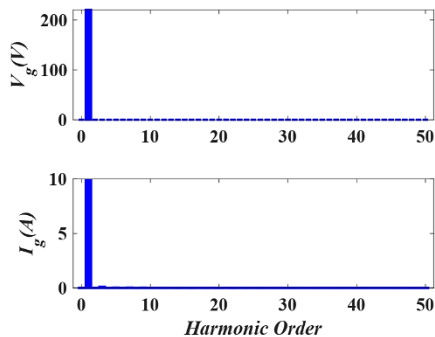


Figure 15. Harmonic spectrum of grid voltage and current during charging mode at 100% battery charge from AC source at power factor = 0.9999, ITHD=2.16%

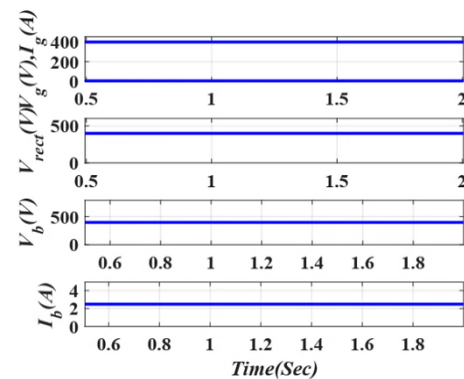


Figure 16. Waveforms during charging mode at 100% battery charge from DC source

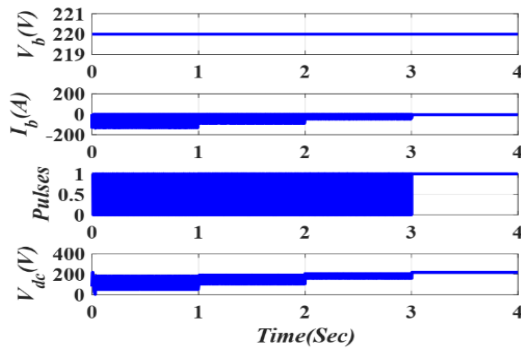


Figure 17. Waveforms during propulsion buck mode for different DC link voltages

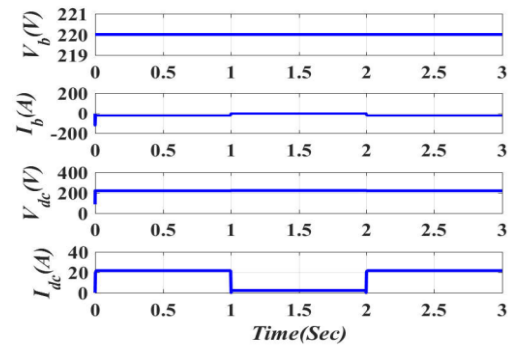


Figure 18. Waveforms during propulsion buck mode with variable load

The waveforms associated during regenerative braking mode by varying DC link voltage are given in Figure 20. The DC link voltage is increased linearly from an initial voltage of 220V to 400V between 0 to 2s, maintained constant between 2 to 2.5s and decreased linearly from 400V to 220V between 2.5 to 3s with constant current of 4.5A. The comparative analysis of the proposed converter with the topologies proposed in [14], [15], [17], [18] and [25] in terms of number of switches, diodes, inductors and capacitors used are tabulated in Table 3. In the proposed topology only three switches, three diodes, two inductors and three capacitors are used. The number of switches used in the proposed topology is least in the table except the topology proposed in [15] but [15] includes seven diodes, three inductors and four capacitors that leads to higher cost and losses.

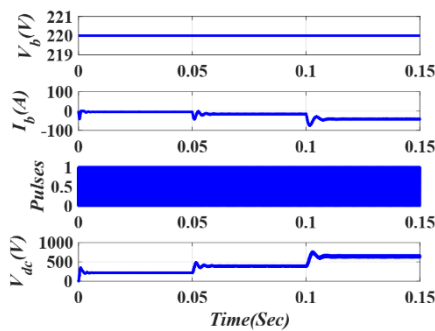


Figure 19. Waveforms during propulsion boost mode at higher speed with change in DC link voltage

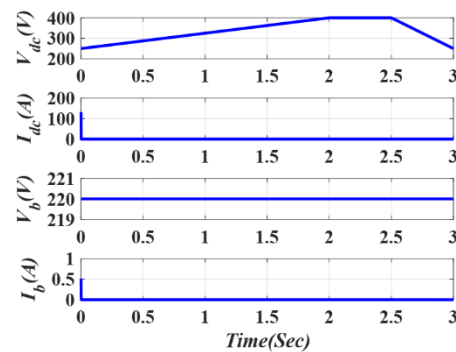


Figure 20. Waveforms during regenerative braking mode

Table 3. Comparison of the proposed topology with existing topologies

Topologies	Switches	Diodes	Inductors	Capacitors	Comments
[14]	4	8	1	1	Slightly higher conduction power loss, efficiency is low.
[15]	6	9	2	2	More conduction losses and low efficiency.
[17]	4	7	2	3	Chances of saturation of core. More Switching losses.
[18]	11	7	1	3	Cost is very high and conduction losses are more.
[25]	3	7	3	4	Passive elements are more.
Proposed topology	3	3	2	3	Number of switches and passive elements are less

6. CONCLUSION

In this paper, single phase multifunctional integrated converter has been proposed for EVs. The proposed topology is operated in plug-in charging with power factor correction mode, propulsion buck and boost mode and regenerative braking mode. In charging mode a power factor of 0.9999 and a current THD of 2.16% is achieved. The proposed topology is compared with the existing topologies in terms of number of switches, diodes, inductors and capacitors and found that the proposed topology uses least switching and passive elements. It means that, higher efficiency, lower cost and small size can be achieved with the proposed topology. Hence, the proposed topology finds immediate applications in EVs manufacturing industries.

REFERENCES

- [1] C Botsford and A. Szczepanek, "Fast charging vs. Slow charging: pros and cons for the new age of electric vehicles," *24th Electric Vehicle Symposium*, Stavanger, Norway, May 2009.
- [2] L. De Sousa, B. Vestre, and B. Bouchez, "A combined multiphase electric drive and fast battery charger for Electric Vehicles," *2010 IEEE Vehicle Power and Propulsion Conference*, 2010, pp. 1-6, doi: 10.1109/VPPC.2010.5729057.
- [3] A. Hassoune, M. Khafallah, A. Mesbahi, A. Nouaiti, and T. Bouragba, "Experimental implementation of a smart battery charger for electric vehicles charging station," *International Journal of Power Electronics and Drive System (IJPEDS)*, vol. 11 no. 4, pp. 1689-1699, Dec. 2020, doi: 10.11591/ijpeds.v11.i4.pp1689-1699.
- [4] S. Kumar and A. Usman, "A Review of Converter Topologies for Battery Charging Applications in Plug-in Hybrid Electric Vehicles," *IEEE Industry Applications Society Annual Meeting*, pp. 1-9, 2018, doi: 10.1109/IAS.2018.8544609.
- [5] K. Liu, X. Hu, Z. Yang, Y. Xie, and S. Feng, "Lithium-ion Battery Charging Management Considering Economic Costs of Electrical Energy Loss and Battery Degradation," *Energy Conversion and Management*, vol. 195, pp. 167-179, Sep. 2019, doi: 10.1016/j.enconman.2019.04.065.
- [6] E. M. Laadissi, J. Khalfi, F. Belhora, C. Ennawaoui, and A. E. Ballouti, "Aging study of a lead-acid storage bank in a multi-source hybrid system," *Indonesian Journal of Electrical Engineering and Computer Science*, vol. 20, no. 3, pp. 1109-1117, Dec. 2020, doi: 10.11591/ijeecs.v20.i3.pp1109-1117.
- [7] K. S. Reddy and S. B. Veeranna, "Design Parameters of Electric Vehicle," *2020 International Conference on Power Electronics & IoT Applications in Renewable Energy and its Control (PARC)*, 2020, pp. 14-21, doi: 10.1109/PARC49193.2020.236548.
- [8] W. Srirattanawichaikul, and P. Wirasant, "Evaluation of lightweight battery management system with field test of electric bus in campus transit system," *International Journal of Electrical and Computer Engineering (IJECE)*, vol. 10, no. 6, pp. 6202-6213, Dec. 2020, doi: 10.11591/ijece.v10i6.pp6202-6213.
- [9] T. Ahmed, H. Kada, and A. Ahmed, "New DTC strategy of multi-machines single-inverter systems for electric vehicle traction applications," *International Journal of Power Electronics and Drive System (IJPEDS)*, vol. 11, no. 2, pp. 641-650, June 2020, doi: 10.11591/ijpeds.v11.i2.pp641-650.
- [10] K. S. Reddy, and B. V. Sreenivasappa, "Review on Power Converters for Electric Vehicles," *Journal of Xi'an University of Architecture & Technology*, vol. 12, no. 8, pp. 82-105, Aug 2020.
- [11] N. Wong and M. Kazerani, "A review of bidirectional on-board charger topologies for plugin vehicles," *IEEE Canadian Conference on Electrical and Computer Engineering (CCECE)*, 2012, pp. 1-6, doi: 10.1109/CCECE.2012.6334957.
- [12] T. Na, X. Yuan, J. Tang, and Q. Zhang, "A review of on-board integrated electric vehicles charger and a new single-phase integrated charger," in *CPSS Transactions on Power Electronics and Applications*, vol. 4, no. 4, pp. 288-298, Dec. 2019, doi: 10.24295/CPSSSTPEA.2019.00027.
- [13] O. C. Onar, J. Kobayashi, D. C. Erb, and A. Khaligh, "A Bidirectional High-Power-Quality Grid Interface With a Novel Bidirectional Noninverted Buck-Boost Converter for PHEVs," in *IEEE Transactions on Vehicular Technology*, vol. 61, no. 5, pp. 2018-2032, Jun. 2012, doi: 10.1109/TVT.2012.2192459.
- [14] S. Dusmez and A. Khaligh, "A Compact and Integrated Multifunctional Power Electronic Interface for Plug-in Electric Vehicles," in *IEEE Transactions on Power Electronics*, vol. 28, pp. 5690-5701, 2013, doi: 10.1109/TPEL.2012.2233763.
- [15] M. Li, Q. Chen, X. Ren, Y. Zhang, K. Jin and B. Chen, "The integrated LLC resonant converter using center-tapped transformer for on-board EV charger," *2015 IEEE Energy Conversion Congress and Exposition (ECCE)*, 2015, pp. 6293-6298, doi: 10.1109/ECCE.2015.7310542.
- [16] Y. Lee, A. Khaligh, and A. Emadi, "Advanced Integrated Bidirectional AC/DC and DC/DC Converter for Plug-In Hybrid Electric Vehicles," in *IEEE Transactions on Vehicular Technology*, vol. 58, no. 8, pp. 3970-3980, Oct. 2009, doi: 10.1109/TVT.2009.2028070.
- [17] A. K. Singh, and M. K. Pathak, "Single-phase bidirectional ac/dc converter for plug-in electric vehicles with reduced conduction losses," *IET Power Electron.*, vol. 11, no. 1, pp. 140-148, Feb 2018, doi: 10.1049/iet-pel.2016.0899.
- [18] M. Mruzek, I. Gajdac, L. Kucera, and D. Barta, "Analysis of Parameters Influencing Electric Vehicle Range," *Procedia Engineering*, vol. 134, pp. 165-174, May. 2015, doi: 10.1016/j.proeng.2016.01.056.
- [19] M. I. Fadzrizan, M. Hanif, M. H. Suid, and M. A. Ahmad, "A piecewise affine PI controller for buck converter generated DC motor," *International Journal of Power Electronics and Drive System (IJPEDS)*, vol. 10, no. 3, pp. 1419-1426, Sep 2019, doi: 10.11591/ijpeds.v10.i3.pp1419-1426.
- [20] M. Hassan *et al.*, "Lyapunov based adaptive controller for power converters used in hybrid energy storage systems," *Sustainable Energy Technologies and Assessments*, vol. 42, Dec. 2020, doi: 10.1016/j.seta.2020.100853.
- [21] R. Pramanik, and B. B. Pati, "Modelling and control of a non-isolated half-bridge bidirectional DC-DC converter with an energy management topology applicable with EV/HEV," *Journal of King Saud University - Engineering Sciences*, Mar. 2021, doi: 10.1016/j.jksues.2021.03.004.
- [22] B. Ge, L. Chen, and S. Zarei, "Model Prediction Based Boost Converter Control Method for HEV Applications," *SAE International in United States*, Apr. 2018, doi: 10.4271/2018-01-0452.
- [23] K. S. Reddy and S. B. Veeranna, "Integrated buck and boost converter for a universal battery charger of an Electric Vehicle," *3rd International Conference on Design and Manufacturing Aspects for Sustainable Energy (ICMED-ICMPC 2021) E3S Web of Conference*, vol. 309, Sep. 2021, doi: 10.1051/e3sconf/202130901073.
- [24] N. Saxena, I. Hussain, B. Singh, and A. L. Vyas, "Implementation of a Grid-Integrated PV-Battery System for Residential and Electrical Vehicle Applications," in *IEEE Transactions on Industrial Electronics*, vol. 65, no. 8, pp. 6592-6601, Aug. 2018, doi: 10.1109/TIE.2017.2739712.
- [25] A. K. Singh, and M. K. Pathak, "Single stage Zeta Sepic Based multifunctional integrated converter for plug-in electric vehicles," *IET Electrical Systems in Transportation*, vol. 8, no. 2, pp. 101-111, May 2018, doi: 10.1049/iet-est.2017.0063.